Quasi-static thermo-electro-mechanical behaviour of piezoelectric stack actuators

Article *in* Smart Materials and Structures · January 2008

DOI: 10.1088/0964-1726/17/1/015049

4 authors, including:

Faxin Li
Peking University
141 PUBLICATIONS **1,651** CITATIONS

Nimal Rajapakse
Simon Fraser University
230 PUBLICATIONS **5,539** CITATIONS

M. S. Gadala
University of British Columbia - Vancouver
145 PUBLICATIONS **2,398** CITATIONS

IOP PUBLISHING SMART MATERIALS AND STRUCTURES

Smart Mater. Struct. **17** (2008) 015049 (10pp) doi:10.1088/0964-1726/17/1/015049

Quasi-static thermo-electro-mechanical behaviour of piezoelectric stack actuators

F X Li[1], R K N D Rajapakse[1,3], D Mumford[2] and M Gadala[1]

[1] Department of Mechanical Engineering, University of British Columbia, 2054-6250 Applied Science Lane, Vancouver, V6T 1Z4, Canada
[2] Westport Power Incorporated, 101-1750 West 75th Avenue, Vancouver, V6P 6G2, Canada

E-mail: rajapakse@mech.ubc.ca

Received 6 June 2007
Published 17 January 2008
Online at stacks.iop.org/SMS/17/015049

Abstract
Quasi-static thermo-electro-mechanical performance of annular and solid cylindrical piezoelectric actuators was studied by experimental means under electric fields varying from 0.3 to 1.8 kV mm^{-1} with a preload of 4.6 MPa over the temperature range of −30 to 125 °C. It was found that, for both annular and solid actuators, the electrically induced stroke increases steadily with temperature. Under electric fields larger than 1.0 kV mm^{-1}, a nonlinear transition zone exists in the stroke–temperature plot over the temperature range 25–50 °C. The dielectric constant was also found to increase with temperature. Preload dependence of displacement was measured up to 42 MPa at room temperature and found to be negligible below 30 MPa. A mathematical model that includes the linear piezoelectric effect and 90° domain switching effect was used to model the experimental results. The model shows reasonable agreement with experimental results at low and high driving fields.

(Some figures in this article are in colour only in the electronic version)

1. Introduction

Piezoelectric ceramics have played an important role in actuator applications due to their excellent electromechanical coupling properties and ultra-fast response [1]. Piezoelectric actuators can generally be classified into two categories [2–4], i.e. (a) rigid displacement devices, for which the strain is induced uni-directionally along an applied direct current (dc) or pulse field, such as servo displacement positioners and actuators of dot-matrix printers, etc; and (b) resonating displacement devices, for which the alternating strain is excited by an alternating current (ac) field at the mechanical resonance frequency, such as ultrasonic piezomotors. The development of co-fired multi-layer technology has made it possible to generate a relatively large displacement in a piezoceramic stack actuator with a low driving voltage. Because they offer quick response, compactness and low power consumption, piezoelectric stack actuators are being investigated for fuel injection systems in the automotive industries and are considered a very competitive candidate for next-generation fuel injectors for clean engine technology [5, 6].

[3] Author to whom any correspondence should be addressed.

The stroke–electric field relationship of piezoelectric actuators over the desired operating temperature range (typically −30 to 125 °C) of automotive fuel injectors and fatigue behaviour under repeated thermo-electro-mechanical loading are critical issues that need to be examined to facilitate further development of fuel injector technology based on piezoelectric actuators. With regard to piezoelectric sensors or motors for high-frequency vibration that work under a low electric field and a low mechanical load, there has been a good deal of experimental data [7, 8] and theoretical studies [9–11] already reported in the literature. However, such studies are of limited value for the development of piezoelectric-actuator-based fuel injector technology as the relevant frequency range for injector applications is low to moderate (10–10^3 Hz), the electric field is high and unipolar (>1.5 kV mm^{-1}) and the operating temperature range is relatively large (typically from −30 to 125 °C). Another important factor is the presence of many material interfaces in a stack actuator that can significantly alter the failure modes when compared to a bulk piezoelectric material. The performance of bulk piezoelectric ceramics under large electric fields was investigated by many researchers, including the nonlinear constitutive behaviour under high

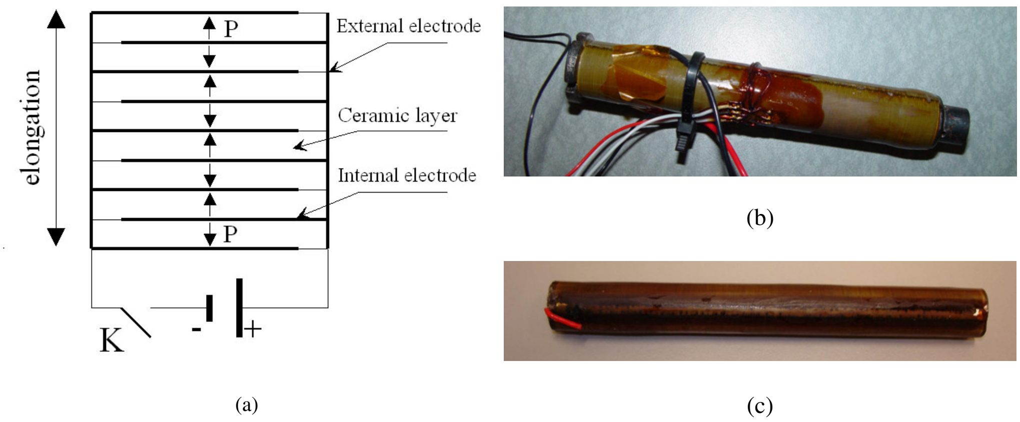

Figure 1. (a) Schematic of a piezoelectric stack actuator (electrodes are denoted by bold lines, the arrow P denotes polarization); (b) instrumented annular actuator; (c) solid actuator.

stresses [12, 13], high stresses coupled with large electric fields [14–16], large electric fields coupled with temperature effects [17–19] and fully coupled thermo-electro-mechanical loading [20]. Electromechanical properties and fatigue behaviour of piezoelectric actuators was also studied [21–24]. However, studies dealing with the performance of piezoelectric multilayer actuators under conditions directly applicable to fuel injector applications do not appear in the literature so far. Such studies are important to the optimum design of injectors and selection of engine operating parameters.

This study therefore investigates the performance of piezoelectric stack actuators for potential use in advanced fuel injectors. It is conducted under conditions as close as possible to the operating loads of automotive fuel injectors. This paper reports the results of an experimental study of quasi-static thermo-electro-mechanical performance of hollow and solid piezoelectric multi-layer actuators and a comparison with a simple mathematical model based on the linear piezoelectric effect and 90° domain switching.

2. Experimental programme

Piezoelectric epoxy-bonded multilayer actuators of two shapes—annular cylindrical and solid cylindrical, manufactured by Kinetic Ceramics Inc. (www.kineticceramics.com)—were used in the experimental investigation. The actuators are made of soft PZT ceramics, with their Curie temperature above 360 °C. The annular cylindrical structure is advantageous with respect to heat dissipation and is also compatible with the design of fuel injectors. Stress concentration in such actuators may be high especially when the preload is large [25]. Figure 1(a) shows the schematic of a stack actuator with the arrangement of electrodes and piezo stacks, and figures 1(b) and (c) show an instrumented annular actuator and a solid actuator used in the present study, respectively. A cylindrical stack actuator consists of N identical piezoelectric thin discs with adjacent discs having opposite poling directions bonded together and electrodes placed between the adjacent discs. Each disc experiences an elongation when a voltage is applied to the electrodes and the actuator stroke is equal to $N\Delta l$ where Δl is the elongation of an individual disc. The properties of the two types of actuators are given in table 1. The actuators chosen in this study are potential candidates for implementation in a fuel injector for clean engine technology.

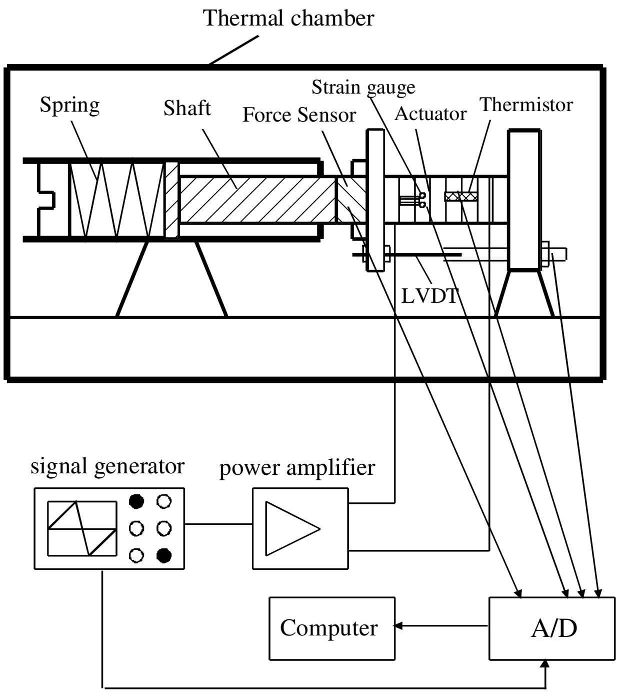

Figure 2. Experimental set-up for quasi-static testing of piezoelectric actuators.

The test set-up is shown in figure 2 and the testing was conducted in a thermal chamber with the temperature controlled to 0.1 °C. A thermistor was bonded to the surface of the actuator to measure the actual temperature of the actuator during testing. An arbitrary driving field can be applied to the actuator by a programmable signal generator and a high-power amplifier. The stroke of the actuator was measured by a high resolution (0.1 μm) linear variable differential transformer (LVDT) mounted between two parallel loading plates that were

Table 1. Properties of KCI annular and solid cylindrical actuators.

Actuator shape	Annular cylinder	Solid cylinder
Actuator diameter (mm)	$D_{out} = 13.7$, $D_{in} = 7.5$	10
Actuator electrode area (mm^2)	97	70
Actuator length (mm)	98.5	93
Active length (mm)	84.2	90.8
Layer thickness (mm)	0.25	0.25
Number of layers	306	330
Capacitance (μF)	1.56	1.23
Full operation voltage (V)	450	450
Full operation electric field (kV mm^{-1})	1.8	1.8
d_{33} (pC N^{-1})	370	
Young's modulus Y_{33}^E (GPa)[a]	48	

[a] Value for the PZT material, not for the actuators.

in tight contact with the actuator. For comparison, the strain of the actuator was also measured with four strain gauges bonded to opposite locations on the actuator surface. The strain gauge readings were collected using a Vishay signal-conditioning amplifier. Preload was applied through a compressive spring and was measured with a force sensor. The driving field, LVDT, thermistor and force sensor signals were input into a data acquisition system and were monitored simultaneously by a computer.

3. Experimental results and discussion

Figure 3 shows the typical waveforms of the recorded voltage, stroke and force during the tests. As shown in figure 3, a trapezoidal-shaped voltage waveform was applied to the actuator with a holding time of 1 s at maximum voltage. Stroke creep during the holding time was about 2–3% and the maximum value of the stroke waveform was considered the stroke corresponding to the maximum voltage level. In the case of a soft preload spring ($k = 30$ N mm^{-1}), the force variation during the activation of the actuator was about 15 N, leading to preload perturbations of only about 0.15 MPa for the annular actuator and 0.2 MPa for the solid one. No detectable temperature change of the actuator was observed during testing.

3.1. Results for annular actuator

The stroke hysteresis of the annular piezoelectric actuators during electrical loading and unloading was first measured by using strain gauges and LVDT. The aim of this testing was to check the validity of the strain gauge results for stroke measurement, thus allowing strain gauges as an option in the event of any difficulty associated with mounting of the LVDT. Figure 4 shows the typical stroke hysteresis of an annular actuator measured at 25 °C by using the LVDT and strain gauges. The preload supplied by the soft spring is equal to 4.6 MPa with the perturbations during testing limited to less than 3%. Hereafter the same preload magnitude is used unless specified otherwise. It can be seen from figure 4 that the strain gauge results agree closely with the LVDT results. In addition, the experimental results show that stroke hysteresis and a zero point drift exist for piezoelectric actuators. The zero point drift usually disappears after one cycle of electric loading, while the stroke hysteresis remains for subsequent loading cycles.

Stiffness testing of both short circuit and open circuit modes was conducted on the annular actuator at room temperature using only strain gauges. The measurement with the LVDT in this case was problematic because the movement of the loading head, to which the LVDT is fixed, was perturbed by the spring during manual loading. The stiffness testing results are shown in figure 5, where two cycles of loading–unloading curves are measured under both short and open circuit conditions. It can be seen from figure 5 that the stiffness for the short circuit condition, 29.4 GPa, is about 1/2 of that for the open circuit condition, 58.7 GPa, which is consistent with previously reported results [26, 27] and the following theoretical relations [9]:

$$1/s_{33}^E = Y_{33}^E = (1 - K_{33}^2)Y_{33}^D = (1 - K_{33}^2)/s_{33}^D \quad (1)$$

where s_{33}^E and s_{33}^D are flexibility coefficients for the short circuit and open circuit conditions, respectively; Y_{33}^E and Y_{33}^D are Young's modulus for the short circuit and open circuit conditions, respectively; K_{33} is the longitudinal electromechanical coupling coefficient, $K_{33} = d_{33}/\sqrt{k_{33}^T s_{33}^E}$, where d_{33} is the longitudinal piezoelectric coefficient and k_{33}^T is the free dielectric coefficient.

Temperature dependence of the dielectric constant and dielectric loss of the annular actuator was measured at 100 Hz, 1 kHz and 10 kHz with a high-resolution impedance analyser LCR817 and is shown in figure 6. It can be seen that, within the testing temperature range of −30 to 125 °C, the dielectric constant increases almost linearly with the temperature and shows a minor dependence on the frequency, which is consistent with the experimental results of Wang *et al* [19]. Zhang *et al* [28] attributed the increasing values of the dielectric constant with temperature to the extrinsic contribution by the increased mobility of both 180° and non-180° domain walls at high temperatures. The dielectric constant is found to slightly decrease with increasing frequency, which is a typical characteristic of dielectric/ferroelectric materials [29, 30]. Under high frequencies, the extrinsic contributions with larger relaxation times cease to respond, leading to a small decrease in the dielectric constant.

The dielectric loss at 100 Hz and 1 kHz remains almost constant (around 2.5%) over the temperature range −30 to

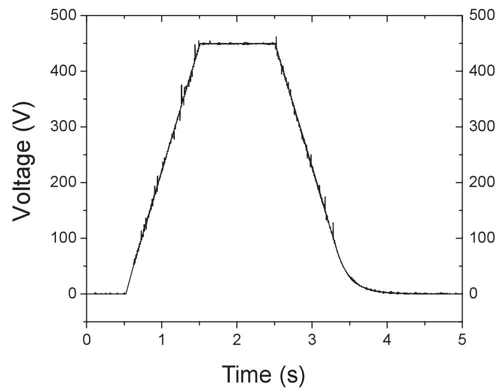

(a) Voltage

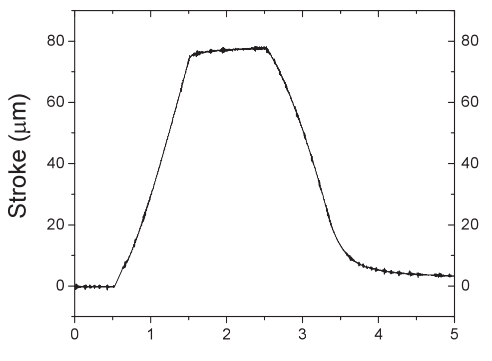

(b) Stroke

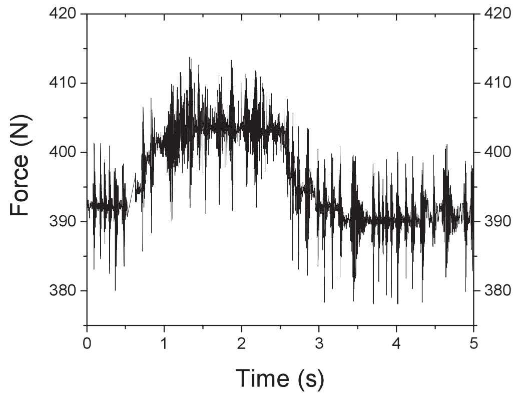

(c) Force

Figure 3. Waveforms of monitored (a) voltage, (b) stroke and (c) force during a typical test.

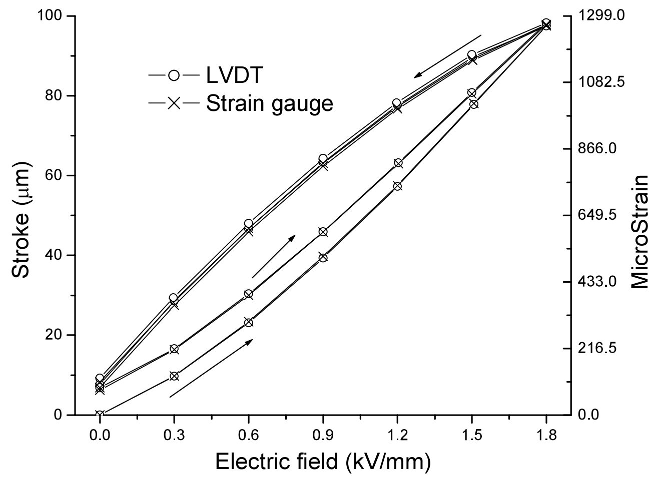

Figure 4. Stroke hysteresis of annular cylindrical actuators measured at 25 °C with LVDT and strain gauges (preload is 4.6 MPa).

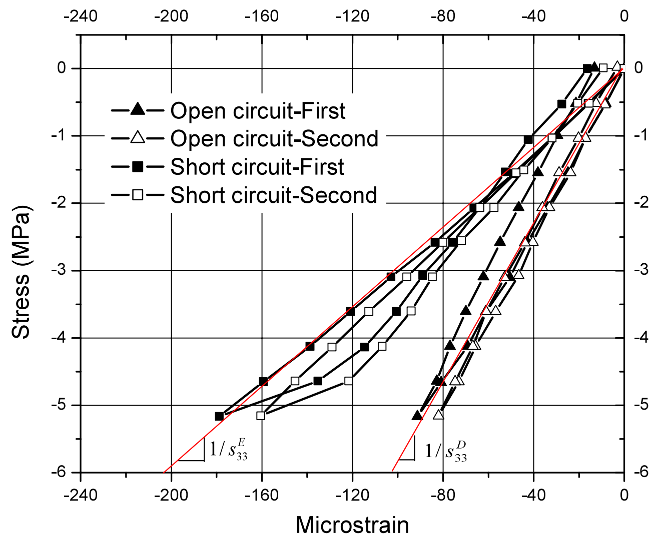

Figure 5. Two cycles of stress–strain curves of annular piezoelectric actuators under open and short circuit conditions.

50 °C. Then it attains a minimum near 100 °C and thereafter shows an increasing trend with temperature. This behaviour qualitatively agrees with the experimental results of Yimnirun *et al* [29] and Sherrit *et al* [31]. As the frequency increases, the trough of the dielectric loss curve is also shifted to a higher temperature, which is consistent with the experimental results by Yimnirun *et al* [29]. If the temperature continues to increase towards the Curie point, then both the dielectric constant and loss reach their peak values [29], but this cannot be realized in the present study because depolarization may occur under high temperature. The relatively large dielectric loss of the actuator also implies that its operation at high frequencies may be prohibited because of considerable heat generation.

Strain gauge measurements were found to become inaccurate at high temperatures (above 50 °C) as the strain reading was obviously smaller than the normally expected value. This is because the strain gauge was not bonded directly to the surface of the ceramic layers, but to the epoxy coating of the piezoelectric actuator. As the temperature rises, the epoxy becomes softer. This softening means that the strain at the outer surface of the epoxy does not accurately reflect the actual strain of the ceramic material, i.e. the strain gauge measurement is inaccurate at temperatures above room level. At room temperature and possibly at lower temperatures, the epoxy is stiff enough that the strain gauge measurement is accurate. In the ensuing sections of the paper, unless specified otherwise, all stroke measurements correspond to results obtained from the LVDT and the strains were calculated from these results.

Figure 7 shows the temperature dependence of the stroke of the annular actuator measured under the trapezoidal driving field (figures 3(a)) with the peak amplitude varied from 0.3 to

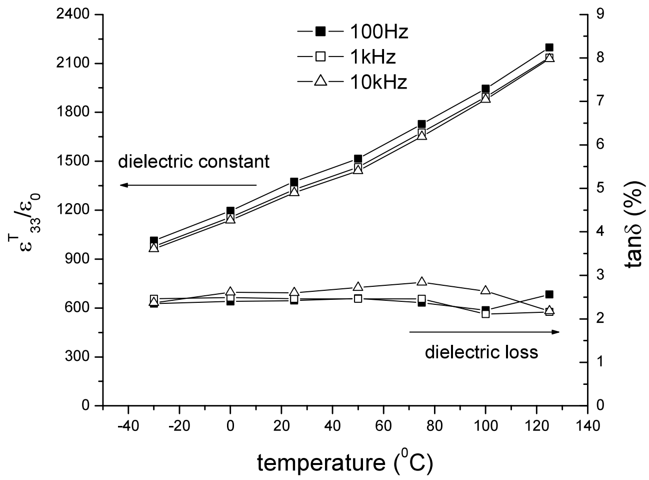

Figure 6. Dielectric constant and dielectric loss of annular actuators at different temperatures and frequencies.

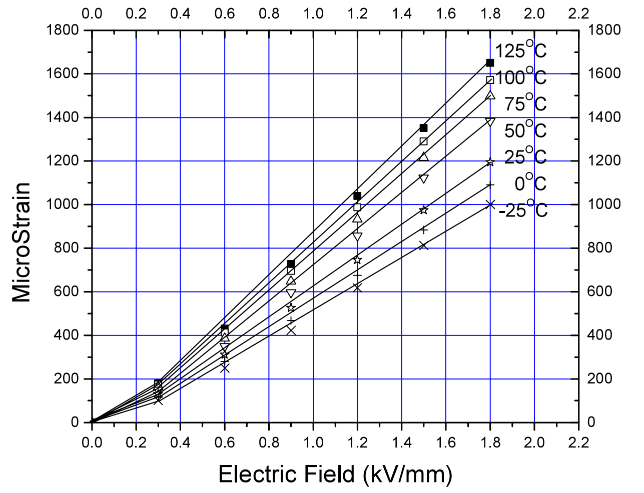

Figure 8. Variation of the stroke of the annular actuator with applied field magnitude and temperature.

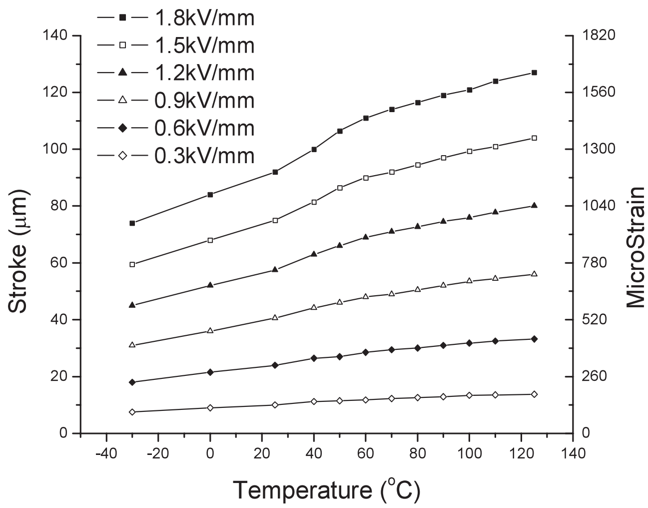

Figure 7. Temperature dependence of the stroke of the annular actuator under different driving field magnitudes.

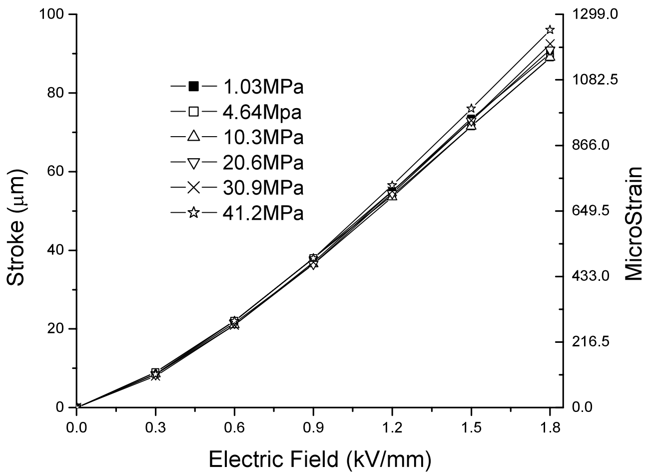

Figure 9. Preload dependence of the stroke of the annular actuator at room temperature (15 °C).

1.8 kV mm^{-1}. It can be seen from figure 7 that, under the applied driving field range, the stroke increases steadily with temperature. For driving fields lower than 0.9 kV mm^{-1}, the stroke–temperature curve is almost linear. For driving fields larger than 1.2 kV mm^{-1}, a nonlinear transition zone exists between 25 and 60 °C, leading to a bilinear stroke–temperature curve. The transition zone becomes more significant as the driving field magnitude increases.

Figure 8 shows the dependence of the stroke of the annular actuator on driving field magnitude over the temperature range −25 to 125 °C. At all temperatures, the stroke increases almost linearly with the driving field except for a slope modulation point at 0.3 kV mm^{-1}. The strain–electric field curve can be approximated, therefore, by a bilinear curve with a point of slope modulation at 0.3 kV mm^{-1}. The stroke at the maximum driving field of 1.8 kV mm^{-1} is about 1.7 times the product of the electric field and the longitudinal piezoelectric constant d_{33} measured at a low field, which indicates that under higher driving fields nonlinear effects such as reversible non-180° domain switching-induced strain may exist. As expected from the results shown in figure 7, the slopes of the stroke–electric field curves in figure 8 increase with increasing temperature and a relatively larger increase is noted from 25 to 50 °C.

Piezoelectric actuators used in fuel injectors are subjected to some preload, depending on the injector design. Preload dependence of the stroke of the annular actuator was investigated in the present study by using a stiffer spring ($K = 200$ N mm^{-1}) with the preload varying from 1.03 to 41.2 MPa. The experimental results at room temperature (15 °C) are shown in figure 9. It can be seen from figure 9 that preload dependence of the stroke is almost negligible with only 6% increase corresponding to the maximum preload of 41.2 MPa and maximum electric field (1.8 kV mm^{-1}). The slight increase of the stroke at larger preloads may be due to 90° domain wall movement. Nevertheless, the preload dependence is almost negligible below 30 MPa, which is the level of preload often used in injector design and the present findings are consistent with the results reported by Pan *et al* [20]. Given the minor dependence of the stroke on preload,

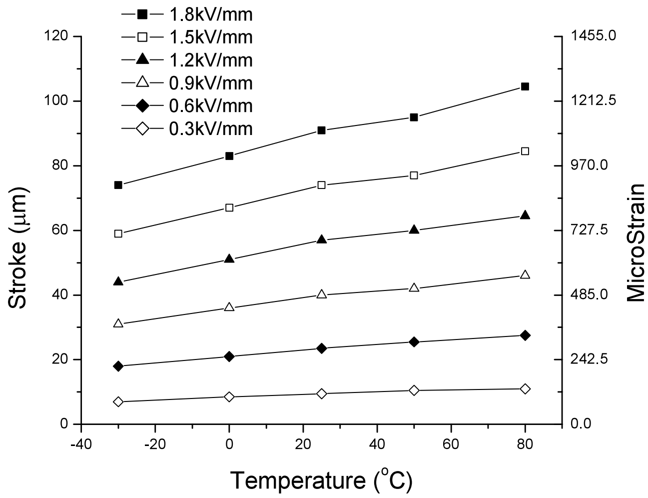

Figure 10. Temperature dependence of the stroke of a solid actuator under different driving field magnitudes.

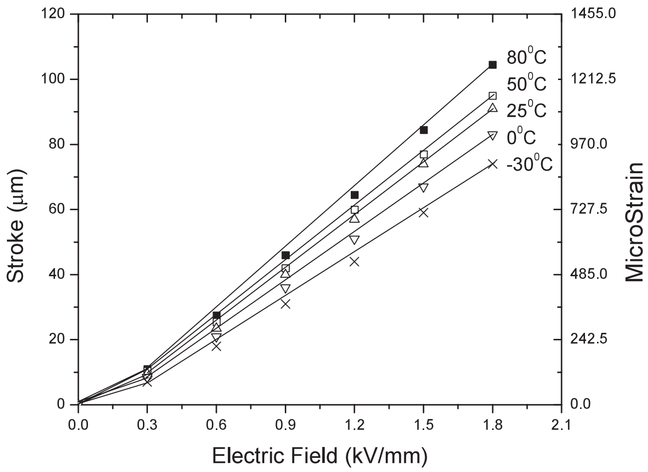

Figure 11. Variation of the stroke of a solid actuator with applied field and temperature.

the preload dependence testing was conducted only at room temperature.

3.2. Results for solid actuator

Solid cylindrical actuators are also used in fuel injector applications. To study the effect of actuator geometry on its performance, further testing was conducted by using solid cylindrical actuators and their properties are given in table 1. It was observed during this series of testing that a custom-made bearing in the test rig might seize at high temperatures and the temperature range was therefore limited to −30 to 80 °C for this series of tests. Figures 10 and 11 show the temperature dependence of the stroke at different driving fields and the driving field dependence of the stroke at different temperatures, respectively. Similar to figures 7 and 8, the stroke increases steadily with temperature and the stroke–electric field relationship is nearly bilinear over the temperature range considered in the present study. The longitudinal strains of the annular actuator at −30 °C are 89 μ and 879 μ for 0.3 kV mm^{-1} and 1.8 kV mm^{-1}, respectively. The corresponding strains of the solid actuator are 77 μ and 815 μ. At 80 °C, the annular actuator strains are 150 μ and 1384 μ for 0.3 kV mm^{-1} and 1.8 kV mm^{-1}, respectively, whereas the corresponding values for a solid actuator are 121 μ and 1151 μ. This shows that the longitudinal strain of the annular actuator is about 10–20% larger than that of the solid actuator under the same applied electric field. Senjuntichai *et al* [32] recently developed a three-dimensional semi-analytical solution for a short piezoelectric cylinder with end electrodes and showed that vertical strain (stroke) increases by nearly 15% with increasing electrode area. Note that, based on table 1, the annular actuator has a comparatively larger electrode area (about 94% of the surface area) than the solid actuator (about 89% of the surface area). In addition, Chen [33] showed that higher field concentrations exist at the two edges of an annular actuator when compared to a solid actuator. Comparatively larger electrode area and higher field concentrations at the edges are the reasons for the 10–20% increase in strain of the annular actuator when compared to a solid actuator.

From figures 7 and 10, it can be seen that the point of slope modulation in the stroke–field plot occurs at the same magnitude of electric field for both annular and solid actuators. However, the convexity of the transition region in the stroke–temperature plot is higher in the case of annular actuators. The preload dependence of the stroke of the solid actuator was measured at room temperature (15 °C) up to 42 MPa and the behaviour is very similar to that of an annular actuator, i.e. the preload dependence of the stroke is almost negligible below 30 MPa.

3.3. Discussion

From the above experimental results, it can be seen that, for both annular and solid actuators, the stroke increases steadily with the temperature and the slopes of stroke–driving field curves increase with temperature. Under a low field, the stroke can be assumed to be completely caused by the linear piezoelectric effect. Zhang *et al* [28] split both the piezoelectric and dielectric constants into intrinsic and extrinsic parts, with the former being properties of a single-domain material and the latter mainly contributed from domain walls, i.e.

$$\varepsilon_{ij} = \varepsilon_{ij}^{\text{in}} + \varepsilon_{ij}^{\text{ex}} \tag{2}$$

$$d_{ij} = d_{ij}^{\text{in}} + d_{ij}^{\text{ex}}. \tag{3}$$

Furthermore, the intrinsic piezoelectric and dielectric responses are related through the electrostrictive coefficient, Q_{ij}, and the remnant polarization, P_{r}, as follows:

$$d_{33}^{\text{in}} = 2\varepsilon_{33}^{\text{in}} Q_{11} P_{\text{r}}. \tag{4}$$

As the intrinsic dielectric constant, $\varepsilon_{33}^{\text{in}}$, is almost independent of temperature and the remnant polarization, P_{r}, decreases slightly with temperature, while the intrinsic piezoelectric constant, d_{33}^{in}, decreases slightly with temperature. On the other hand, the extrinsic piezoelectric constant, d_{33}^{ex}, which is about 70% of the total piezoelectric constant at room temperature [28], increases rapidly with temperature as a result of the increased effects of non-180° domain walls. Thus, the low-field strokes shown in figure 7 and figure 10 increase steadily with temperature.

In the case of a relatively large applied field, assume that the stroke is caused only by the piezoelectric effect and the piezoelectric coefficient is no longer constant, but increases with the applied field. Following Zhang *et al* [28], the effective piezoelectric coefficient can be expressed as

$$d_{33}^{\mathrm{eff}}(E,\sigma,T) = d_{33}^{\mathrm{in}}(T) + d_{33}^{\mathrm{ex}}(T) + \Delta d_{33}^{\mathrm{ex}}(E,\sigma,T) \qquad (5)$$

where E, σ, T are applied electric field, applied stress and temperature, respectively.

The last term, $\Delta d_{33}^{\mathrm{ex}}$, is also an extrinsic response and caused by increased activities of non-180° domain walls under large fields only. It will increase with the applied field/stress and temperature, but vanish under low field/stress. Thus, the stroke increases with temperature and the slopes of stroke–temperature curves in both figures 7 and 10 increase with the applied electric field.

From figure 9, it can be seen that the stroke increases slightly with the applied preload and the differences are noticeable only above 30 MPa and 1.2 kV mm^{-1}. The preload dependence of the stroke can also be explained by equation (5). The increasing preload does not affect the low-field piezoelectric constants (the first two terms), but it increases $\Delta d_{33}^{\mathrm{ex}}$ under a high electric field by making the non-180° domain walls more active. Thus, the high-field stroke tends to increase with the preload as long as the preload does not depolarize the actuator.

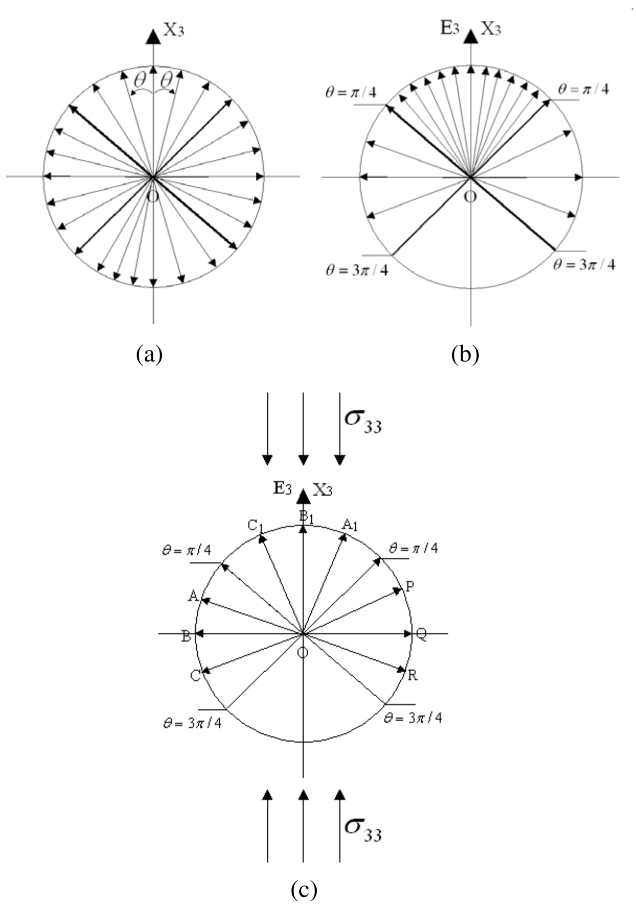

Figure 12. Two-dimensional illustration of domain distribution in tetragonal ferroelectric ceramics: (a) unpoled ceramic; (b) poled ceramic; (c) 90° switchable domains in poled ceramic under applied stress.

4. Mathematical model

In this section, a simple mathematical model is developed to examine the response observed in the experiments. To physically explain the dependence of the stroke on temperature and driving field, it is proposed to divide the stroke into two parts: one part corresponds to linear piezoelectricity and the other is caused by a small fraction of reversible non-180° domain switching under a high electric field. As noted in the discussion of figure 7, the latter part is about 70% of the linear piezoelectric effect for a driving field of 1.8 kV mm^{-1}. Obviously, the temperature dependence of the linear piezoelectric part of the stroke can be obtained directly from the low-field piezoelectric constant d_{33} data measured at different temperatures. As to the latter part of the stroke corresponding to domain switching, it is assumed that the PZT actuator used in the present investigation is tetragonal and thus only 90° domain switching is responsible for this part of the stroke. According to Berlincourt and Krueger [26], in a perfectly poled $PbZr_{0.53}Ti_{0.47}$ ceramic, 180° switching is virtually complete when compared to an unpoled material, while 90° domain orientation is only about 53% complete (49% complete for $PbZr_{0.52}Ti_{0.48}$ doped with 1 wt% Nb_2O_5 as stabilizing agent) with the applied field and about 44% with the field removed. The domain-switching-induced component of the stroke is therefore based on a relatively small fraction (about 5%–9%) of reversible 90° switching.

The domain-switching model used in this paper is based on Li *et al* [34]. In the model, a ferroelectric ceramic is assumed to be composed of numerous crystallites, each of which is a single domain with its distinct polar direction. Furthermore, each crystallite is assumed transversely isotropic around its local polar axis and can only switch in planes parallel to the electric loading direction, i.e. the poling direction. Based on these assumptions, the states of domains can be described by a one-dimensional orientation distribution function (ODF), $f(\theta)$, where $\theta(0 \leqslant \theta \leqslant \pi)$ denotes the angle between the domain local polar vector P and the positive direction of the $\mathbf{X_3}$ axis, as shown in figure 12(a), which is a two-dimensional illustration of domain distribution in an unpoled ferroelectric ceramic. According to Li *et al* [34], the ODF for an unpoled ceramics is

$$f(\theta) = \tfrac{1}{2}\sin\theta \qquad (0 \leqslant \theta \leqslant \pi). \qquad (6)$$

According to Berlincourt and Krueger [26], 180° switching is nearly complete in a poled ceramic, i.e. all domains with the polar orientation angle satisfying $3\pi/4 \leqslant \theta \leqslant \pi$ switch into a $\pi/4$ cone around the poling direction, as shown in figures 12(b). A small fraction of 90° switchable domains, with their polar orientation angle $\theta \in (\pi/4, 3\pi/4)$, are assumed to be distributed uniformly on the spherical zone between $\theta = \pi/4$ and $\theta = 3\pi/4$. Such an assumption is acceptable because only when the constraining stress induced by 90° switching is large enough, can a 90° switched domain switch back to its original state with the electric field removed. It is reasonable to assume that the magnitude of the constraining stress induced by 90° switching is independent of the original polar direction. For a clearer illustration, only a small fraction of 90° switchable domains is shown in figure 12(c), where under a high electric field E_3, domains with original polar vectors OA, OB and OC switch to OA_1, OB_1 and OC_1, respectively. The domains with polar vectors OP, OQ and OR are symmetric with the domains having polar vectors OA, OB and OC.

When a domain undergoes 90° switching, the induced longitudinal spontaneous strain is

$$\Delta\varepsilon_{33}^{s} = \frac{3\gamma_0}{2}(\sin^2\theta - \cos^2\theta). \tag{7}$$

It should be noted that the transversely isotropic domain assumption overestimates the net spontaneous strain due to perfect 90° reorientation in polycrystalline tetragonal ferroelectrics. Referring to Li *et al* [34], the saturated polycrystalline strain under such an assumption is $\frac{\sqrt{2}}{2}\gamma_0$, while the ideal value for a real tetragonal ceramic is $0.368 \times \frac{3}{2}\gamma_0 = 0.552\gamma_0$ [35–37]. To address this difference, a multiplication factor, $\beta = 0.552/(\sqrt{2}/2) = 0.781$, is introduced into equation (7).

In this model, a p fraction of 90° switchable domains (p is about 5%–9%) is assumed to participate in the reversible switching process under a high driving field. The widely accepted domain switching criterion by Hwang *et al* [38] is used to determine whether a domain switches or not. The 90°-switching barrier $W_{90}(T)$ is also temperature-dependent and assumed to be expressed by the product of the coercive field $E_C(T)$ and the spontaneous polarization $P_0(T)$. The coercive field $E_C(T)$ is thought to be similar to that in barium titanate ceramics, decreasing linearly with increasing temperature [36], i.e.

$$E_C(T) = E_C(T_0) + \alpha_E(T - T_0) \tag{8}$$

where T_0 is a given temperature, $E_C(T_0)$ is the coercive field at this temperature and α_E is the slope of the coercive field versus temperature curve.

In the case of figure 12(c), the domain-switching criterion therefore simplifies to

$$E_3P_0(T)(\sin\theta - \cos\theta) - \sigma_{33}3\gamma_0/2(\sin^2\theta - \cos^2\theta) \geqslant E_C(T)P_0(T), \qquad \pi/4 < \theta < 3\pi/4 \tag{9}$$

where $\gamma_0 = \frac{2}{3}(c/a - 1)$ is the longitudinal spontaneous strain of a single domain, with c and a denoting the lattice constants of a tetragonal ferroelectric crystal, and E_3 and σ_{33} are applied electric field and applied stress, respectively.

For PZT, the typical values of the parameters in equation (9) at room temperature are $P_0 = 0.75$ C m^{-2}, $c/a = 1.02$ and $E_C = 1.0$–1.5 kV mm^{-1} [26, 36]. As the measured preload dependence of the stroke in the present study is almost negligible in the event of domain switching under a very low preload ($\sigma_{33} = 4.6$ MPa), the second term on the left-hand side of equation (9) is about one order smaller than the other terms. For simplicity, this term is neglected and equation (9) reduces to

$$E_3(\sin\theta - \cos\theta) \geqslant E_C(T), \qquad \pi/4 < \theta < 3\pi/4. \tag{10}$$

Under a given electric field E_3, assume that θ_c is the critical angle which satisfies equation (10), i.e.

$$E_3(\sin\theta_c - \cos\theta_c) = E_C(T). \tag{11}$$

Obviously the left-hand side of equation (10) is a monotonically increasing function of θ; thus it can be concluded that all possible switchable domains with the polar orientation angle θ between $(\theta_c, 3\pi/4)$ switch to the $\pi/4$ cone around the poling axis. The ODF of these domains is

$$f(\theta) = \frac{p}{2}\sin\theta, \qquad \theta \in (\theta_c, 3\pi/4). \tag{12}$$

The 90° switching-induced longitudinal strain by these domains can be expressed as

$$\Delta\varepsilon_{33} = \int_{\theta_c}^{\frac{3\pi}{4}} \frac{3\gamma_0}{2}\beta(\sin^2\theta - \cos^2\theta)\frac{p}{2}\sin\theta\,\mathrm{d}\theta = \frac{\beta p\gamma_0}{4}(\sqrt{2} + \sin^2\theta_c\cos\theta_c + 2\cos\theta_c - \cos^3\theta_c). \tag{13}$$

For a given electric field E_3 and a prescribed coercive field $E_C(T)$ at different temperatures, after solving θ_c from equation (11), the strain induced by the p fraction of 90° switchable domains can be computed from equation (13).

Figure 13 shows a comparison between the experimental results and simulation results based on the current mathematical model for annular actuators. In the simulations, the required piezoelectric constants are taken from the low field slope of figure 8. The parameters for $E_C(T)$ in equation (8) are

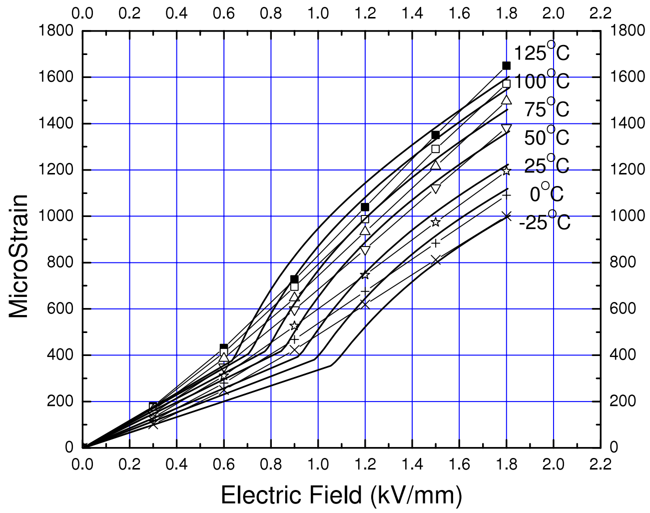

Figure 13. Experimental and theoretical strain–electric field relationship of annular actuators at different temperatures (experimental results—symbols, theoretical results—lines).

$E_C(0\,°C) = 1.4$ kV mm^{-1} and $\alpha_E = -0.004$ kV mm^{-1} °C^{-1} [36]. The fraction p in equation (13) is taken as 7% referring to Berlincourt and Krueger [26]. Note these are only approximate values based on the existing literature and may not exactly correspond to the ceramic used by KCI.

It can be seen from figure 13 that the mathematical model fits quite well with the experimental results at lower driving fields (smaller than 300 V mm^{-1}) and at very high fields (larger than 1.5 kV mm^{-1}). However, at intermediate driving fields, the prediction of the model is not good. This is probably due to the fact that, in the current domain switching model, the intergranular interactions between domains are neglected during switching and the material is thought to be stress-free initially. In a real ceramic, 90° switching induces considerable constraints from the adjacent domains and the initial poled state is usually not stress-free even in the absence of a preload. In addition, the material properties used in the simulations are only approximate values and the effects of complex 3D stress and electric field that exist in an actuator due to various material interfaces are neglected in the present study.

5. Conclusions

Quasi-static thermo-electro-mechanical performance of annular and solid cylindrical piezoelectric actuators was investigated at temperatures, driving fields and preloads that are typical for automotive fuel injector applications. For both types of actuators, the electric-field-induced stroke was found to increase steadily with temperature. Under electric fields larger than 1.0 kV mm^{-1}, a nonlinear transition zone exists in the stroke–temperature plot over the temperature range 25–50 °C. The transition zone becomes more significant for driving fields greater than 1.0 kV mm^{-1}. A clear point of inflection exists in the stroke–driving field plot at 0.3 kV mm^{-1} for all temperatures leading to a bilinear dependence of stroke on the driving field. The dielectric constant was also measured and found to increase almost linearly with temperature. Preload dependence of stroke was measured up to 42 MPa for both types of actuators and was found to be negligible below 30 MPa. A simple mathematical model that includes the linear piezoelectric effect and 90° domain switching effects was used to compare with the experimental results. The model predicts the trends of the experimental results well at lower driving fields (smaller than 300 V mm^{-1}) and at very high fields (larger than 1.5 kV mm^{-1}), but needs improvement for moderate fields.

Acknowledgments

The authors are grateful to Damien Clapa, Charlie Loo and Liam Segarty of Westport Power Inc. for providing assistance during testing. This research was supported by a research grant from the Natural Sciences and Engineering Research Council (NSERC) of Canada with substantial in-kind support provided by Westport Power Inc.

References

[1] Xu Y 1991 *Ferroelectric Materials and their Applications* (Amsterdam: North-Holland)

[2] Uchino K 1996 *Piezoelectric Actuators and Ultrasonic Motors* (Boston, MA: Kluwer)

[3] Uchino K 1998 Materials issues in design and performances of piezoelectric actuators: an overview *Acta Mater.* **46** 3745–53

[4] Uchino K 1998 Piezoelectric ultrasonic motors: overview *Smart Mater. Struct.* **7** 273–85

[5] Jänker P 1997 Electro-mechanical characterization of high-performance piezoactuators *Proc. SPIE Smart Struct. Mater.* **3039** 670–7

[6] Schuh C *et al* 2000 Piezoceramic multilayer actuators for fuel injection systems in automotive area *Proc. SPIE Smart Struct. Mater.* **3992** 165–75

[7] Uchino K, Kato K and Tohda M 1988 Ultrasonic linear motors using a multilayered piezoelectric actuator *Ferroelectrics* **87** 331–4

[8] Funakubo T *et al* 1995 Ultrasonic linear motor using multilayer piezoelectric actuators *Japan. J. Appl. Phys.* **34** 2756–9

[9] Ikeda T 1990 *Fundamentals of Piezoelectricity* (Oxford: Oxford University Press)

[10] Wang X, Ehlers C and Neitzel M 1996 Electro-mechanical dynamic analysis of the piezoelectric stack *Smart Mater. Struct.* **5** 492–500

[11] Ye D and Sun J Q 1997 Dynamic analysis of piezoelectric stack actuators including thermal and pyroelectric effects *Proc. SPIE Smart Struct. Mater.* **3039** 619–29

[12] Krueger H H A 1967 Stress sensitivity of piezoelectric ceramics: part 1. Sensitivity to compressive stress parallel to the polar axis *J. Acoust. Soc. Am.* **42** 636–45

[13] Schaufele A B and Hardtl K H 1996 Ferroelastic properties of lead zirconate titanate ceramics *J. Am. Ceram. Soc.* **79** 2637–40

[14] Lynch C S 1996 The effect of uniaxial stress on the electro-mechanical response of 8/65/35 PLZT *Acta Mater.* **44** 4137–48

[15] Fang D N and Li C Q 1999 Nonlinear electric-mechanical behavior of a soft PZT-51 ferroelectric ceramic *J. Mater. Sci.* **34** 4001–10

[16] Li F X and Fang D N 2005 Effects of lateral stress on the electromechanical response of ferroelectric ceramics: experiments versus model *J. Intell. Mater. Syst. Struct.* **16** 583–8

[17] Zhang Q M, Wang H and Zhao J 1994 Effect of driving field and temperature on the response behavior of ferroelectric actuator and sensor materials *J. Intell. Mater. Syst. Struct.* **6** 84–93

[18] Jiang Q Y, Subbarao E C and Cross L E 1994 Effect of composition and temperature on electric fatigue of La-doped lead zirconate titanate ceramics *J. Appl. Phys.* **75** 7433–43

[19] Wang D, Fotinich Y and Carman G P 1998 Influence of temperature on the electromechanical and fatigue behavior of piezoelectric ceramics *J. Appl. Phys.* **83** 5342–50

[20] Pan M J *et al* 1998 Electroactive actuator materials: investigations on stress and temperature characteristics *Proc. SPIE Smart Struct. Mater.* **3324** 145–53

[21] Zheng J *et al* 1996 Heat generation in multilayer piezoelectric actuators *J. Am. Ceram. Soc.* **79** 3193–98

[22] Sakai T and Kawamoto H 1998 Durability properties of piezoelectric stack actuators *Japan. J. Appl. Phys.* **37** 5338–41

[23] Yao K *et al* 2000 Compact piezoelectric stacked actuators for high power applications *IEEE Trans. Ultrason. Ferroelectr. Freq. Control* **47** 819–25

[24] Mitrovic M, Carman G P and Straub F K 2001 Response of piezoelectric stack actuators under combined electro-mechanical loading *Int. J. Solids Struct.* **38** 4357–74

[25] Rajapakse R K N D, Chen Y and Senjuntichai T 2005 Electroelastic field of a piezoelectric annular finite cylinder *Int. J. Solids Struct.* **42** 3487–508
[26] Berlincourt D and Krueger H H A 1959 Domain processes in lead titanate zirconate and barium titanate ceramics *J. Appl. Phys.* **30** 1804–10
[27] Li F X and Fang D N 2005 Effect of electrical boundary conditions and poling approaches on the mechanical depolarization behavior of PZT ceramics *Acta Mater.* **53** 2665–73
[28] Zhang Q M *et al* 1994 Direct evaluation of domain-wall and intrinsic contributions to the dielectric and piezoelectric response and their temperature dependence on lead zirconate–titanate ceramics *J. Appl. Phys.* **75** 454–9
[29] Yimnirun R, Ananta S and Laoratanakul 2004 Effects of Pb(Mg1/3Nb2/3)O3 mixed-oxide modification on dielectric properties of Pb(Zr0.52Ti0.48)O3 ceramics *Mater Sci. Eng.* B **112** 79–86
[30] Rai R, Sharma S, Soni N C and Choudhary R N P 2006 Investigation of structural and dielectric properties of (La, Fe)-doped PZT ceramics *Physica* B **382** 252–6
[31] Sherritt S, Yang G, Wiederick H D and Mukherjee B K 1999 Temperature dependence of the dielectric, elastic and piezoelectric material constants of lead zirconate titanate ceramics *Proc. Int. Conf. on Smart Materials, Structures, and Systems* pp 121–6
[32] Senjuntichai T, Kaewjuea W and Rajapakse R K N D 2008 Piezoelectric cylinder under voltage and mechanical loading *Int. J. Appl. Electromagn. Mech.* **27** 93–116
[33] Chen Y 2003 Analysis of piezoelectric cylindrical actuators and 1-3 piezocomposite unit cells *MASc Thesis* The University of British Columbia, Canada
[34] Li F X, Fang D N and Soh A K 2004 An analytical axisymmetric model for the poling-history dependent behavior of ferroelectric ceramics *Smart Mater. Struct.* **13** 668–75
[35] Baerwald H G 1957 Thermodynamic theory of ferroelectric ceramics *Phys. Rev.* **105** 480–6
[36] Jaffe B, Cook W R and Jaffe H 1971 *Piezoelectric Ceramics* (London: Academic) p 17
[37] Li F X and Rajapakse R K N D 2007 Analytical saturated domain orientation textures and electromechanical properties of ferroelectric ceramics due to electric/mechanical poling *J. Appl. Phys.* **101** 054110
[38] Hwang S C, Lynch C S and McMeeking R M 1995 Ferroelectric/ferroelastic interactions and a polarization switching model *Acta. Metall. Mater.* **43** 2073–84